Geological Society of America
Special Paper 407
2006

Synrift geometry of the Neuquén Basin in northeastern Neuquén Province, Argentina

Ernesto Cristallini*
Laboratorio de Modelado Geológico (LaMoGe), Departamento de Ciencias Geológicas, FCEyN, Universidad de Buenos Aires (Consejo Nacional de Investigaciones Científicas y Técnicas), Ciudad Universitaria, Pabellón 2, 1428 Buenos Aires, Argentina
Germán Bottesi
Alejandro Gavarrino
Leonardo Rodríguez
Repsol YPF, Diagonal Roque Saenz Peña 777, (1035), Buenos Aires, Argentina
Renata Tomezzoli
Instituto de Geomagnetismo "Daniel Valencio," Departamento de Ciencias Geológicas, FCEyN, Universidad de Buenos Aires (Consejo Nacional de Investigaciones Científicas y Técnicas), Ciudad Universitaria, Pabellón 2, 1428 Buenos Aires, Argentina
Raúl Comeron
Repsol YPF, Diagonal Roque Saenz Peña 777, (1035), Buenos Aires, Argentina

ABSTRACT

A map of the principal grabens and half-grabens of the Neuquén Basin in the northeastern part of Neuquén Province, Argentina, was constructed based on two-dimensional (2-D) and three-dimensional (3-D) seismic information. The synrift structure of the region is characterized by high angle NW-trending normal faults. Two populations can be distinguished: one with an azimuth of 140° and the other one with an azimuth of 105°. The principal half-grabens are accommodated by NE-dipping normal faults. The principal NW-trending faults are less than 20 km long and are either crosscut by or terminate in transfer zones trending to the NE. The transfer zones are either faults or zones where the principal NW-trending faults loose slip or terminate. The principal normal faults were active until the deposition of the Lower Upper Jurassic Tordillo Formation. Subsequently, only a few faults related to differential subsidence over the half-grabens remained active. The typical structures of the region are smooth anticlines and synclines that affect the sag facies of Neuquén Basin. The anticlines developed over basement highs and the synclines over graben basins. The synclines are explained in this study as resulting from differential subsidence over the half-grabens. This differential subsidence could have been a continuous process that began in the synrift stage of the basin. A distinct element model was

*E-mail: ernesto@gl.fcen.uba.ar.

Cristallini, E., Bottesi, G., Gavarrino, A., Rodríguez, L., Tomezzoli, R., and Comeron, R., 2006, Synrift geometry of the Neuquén Basin in northeastern Neuquén Province, Argentina, *in* Kay, S.M., and Ramos, V.A., eds., Evolution of an Andean margin: A tectonic and magmatic view from the Andes to the Neuquén Basin (35°–39°S lat): Geological Society of America Special Paper 407, p. 147–161, doi: 10.1130/2006.2407(07).

created out to analyze the differential subsidence process and geometry. No evidence was found to support the hypothesis that tectonic inversion is an important process in this region. The main unconformities can be explained by the differential subsidence process.

Keywords: Neuquén Basin, differential subsidence, rifting, Entre Lomas Height.

INTRODUCTION

The Neuquén Basin is a retroarc rift-related basin in southwestern South America that has developed since Triassic times (Fig. 1). Synrift sequences were deposited until the middle of the Jurassic and were followed by typical sag phase sequences, which were deposited up until Upper Cretaceous time. Tectonic inversion associated with the Andean orogeny began in the Upper Cretaceous on the western side of the basin, with continental sediments accumulating in the foreland. Earlier episodes of inversion in the Jurassic in the southern part of the basin can be related to strike-slip and wrench tectonics (Dorsal de Huincul area; Orchuela et al., 1981; Ploszkiewicz et al., 1984; Bettini, 1984).

The Neuquén Basin is the most important Argentine basin in terms of hydrocarbon production, accounting for nearly half of the oil and gas produced in the country. In this paper, we analyze the northeastern region of the basin, which is one of the most important areas for oil and gas production. The northeastern border of the basin developed over a first-order crustal discontinuity (Dalmayrac et al., 1980; Ramos 1984, 1988; Tomezzoli, 2001). This discontinuity controlled the Triassic synrift structures in the northeastern part of the basin (Ramos, 1984).

The oil fields of this area have an important structural control (Veiga et al., 1999) related to the principal faults that bound the Triassic half-grabens. These NW-trending faults define anticlinal highs and synclinal troughs in all of the post-Triassic sedimentary sequences. These structural highs and lows also exert a control on the modern topography and drainage. An important question is why the Triassic structures control the subsequent

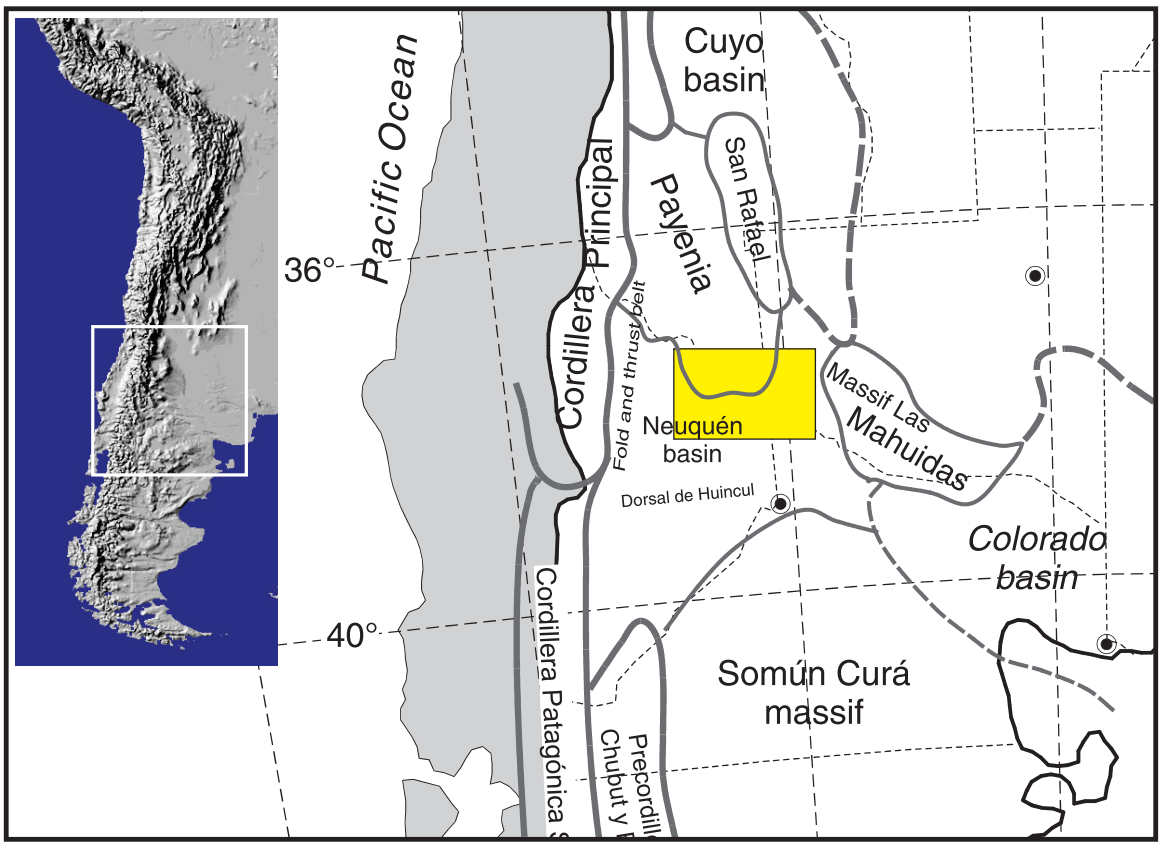

Figure 1. Location map of the Neuquén Basin and the neighboring geological provinces of southern Argentina. The area considered in this study is shown in the boxed region, which corresponds to the region shown in Figure 2.

sedimentary history of the region. Is tectonic inversion controlling the structure in this region, as is the case in the western and southern parts of the Neuquén Basin? Is extensional reactivation of Triassic structures playing a role? Or is the main control differential subsidence?

In this paper, we present an integrated map based on two-dimensional (2-D) and three-dimensional (3-D) seismic information that shows the arrangement and geometry of the principal Triassic half-graben structures of the northeastern Neuquén Basin. We then analyze the mechanism by which the basement structures are controlling the sedimentation and structure of the uppermost portion of the sedimentary cover.

OBSERVATIONS

Map of Principal Synrift Faults

A main objective in this investigation was the construction of a regional map of the principal grabens and half-grabens of the Neuquén Basin in the northeastern part of Neuquén Province. The principal data used were several 2-D seismic lines from the Repsol YPF company. Some 3-D seismic and borehole information were used as a check in specific regions.

The map of the principal graben and half-graben structures is shown in Figure 2. The faults are categorized according to importance, with their relative importance indicated by the

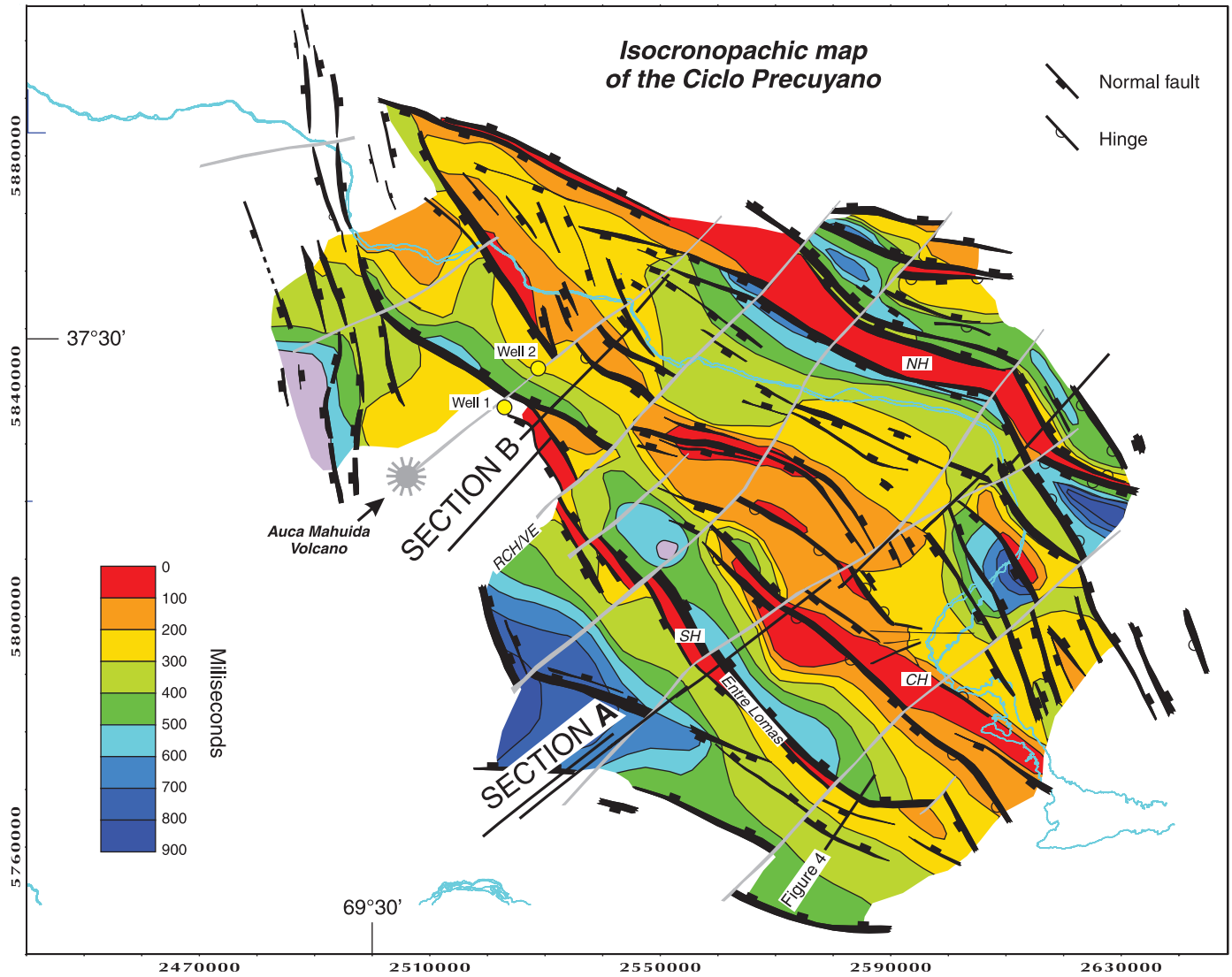

Figure 2. Map of the principal grabens and half-grabens of the region. Colors represent seismic thickness measured in two-way travel time (TWT) units (ms) of pre-Cuyo Group deposits. RCH/VE—Rincon Chico–Veta Escondida lineament. The northern (NH), central (CH) and southern (SH) highs discussed in the text are shown. Locations of the cross-sections A and B are indicated. The trace thickness used to represent faults and hinges is proportional to the half-graben and fault importance (see reference on text). Map is based on the Gauss-Kruger coordinate system (Argentina-zone 2) using the Campo Inschauspe Datum; units are meters.

thickness of the fault trace. The importance of a fault is a subjective characteristic and can change during the history of the fault. In this paper, we consider the importance of each fault only for the synrift stage of the basin. The variables used to calculate the importance of a fault are: (1) In cases where the fault represents the boundary of a graben or half-graben, the thickness of synrift deposits was considered as the most sensitive parameter in determining importance. (2) In cases where the fault does not represent the boundary of a graben or half-graben (i.e., internal faults of a half-graben), the slip of the fault was considered as the most sensitive parameter in determining importance. (3) A subjective value was assigned based on the aspect of the fault in the seismic line.

The following equation was used in the calculation of the importance of each fault:

$$I = (T \times K_T + S \times K_S)V, \quad (1)$$

where I is the importance of the fault, T is the parameter representing the thickness of the graben or half-graben (with values from 1 to 8), S is the parameter representing the slip of the fault (with values from 1 to 8), V is the subjective parameter assigned according to the aspect of the fault in the seismic lines (with values from 1 to 3), and K_T and K_S are Boolean variables. The value of K_T is 1 in number (1) situations and 0 in number (2) situations, and the value of K_S is 1 in **b** cases and 0 in **a** cases. The thickness of the fault traces in Figure 2 is proportional to I.

The summary map in Figure 2 shows that the synrift faults have high dip angles and generally trend to the NW. Two populations are present, one with an average azimuth of 140° and the other with an average azimuth of 105°. Overall, 52% of the analyzed faults dip to the SW and 48% dip to the NE. The most important half-graben system in the region is located just to the northeast of the Entre Lomas high and is bounded by NE-dipping faults. There is no relation between trend populations and dip directions.

Transfer zones with NE trends were also identified and mapped in Figure 2. The transfer zones are defined by aligned sectors where the main faults lose continuity. In a few cases, they are represented by NE-trending faults. One of these transfer zones coincides with the Rincón Chico–Veta Escondida alignment described by Veiga et al. (1999). Transfer zones can exert an important control on surface features, as shown by the position of the Auca Mahuída volcanic complex and some of the sharp curves of the Colorado River.

The map in Figure 2 shows half-graben configurations at the end of the pre-Cuyo Group synrift in the Lower Jurassic. Thicknesses of synrift deposits are denoted by the corresponding seismic (two-way travel) time interval (isocronopachic map). Three main highs are observed and designated as the northern high, the southern high, and the central high. The northern high (NH in Fig. 2) is an 8-km-wide and 100-km-long horst located near the northeast boundary of the Neuquén Basin. It is a symmetric NW-trending structure bounded by NE-dipping faults to the north and SW-dipping faults to the south. The southern high (SH in Fig. 2) is equivalent to the Entre Lomas–Señal Cerro Bayo (Veiga et al., 1999) lineament and corresponds to a NW-trending horst. It is a clear asymmetric structure where the main fault bounds the structure to the north and dips northeast. The horst is limited to the south by a less important, SW-dipping fault. Compared to the northern high, the southern high is similar in length, narrower, and more fragmented by transfer zones. Compared to the other two highs, the central high (CH in Fig. 2) is less important and more complex, in that it is more segmented and branched out. In general, this high is formed by the elevated parts of half-graben footwalls, and some segments have a horst structure.

The principal synrift basin of the region is located between the central and southern highs, and the deepest and best-defined troughs occur in this area. The troughs are asymmetric basins (half-grabens) that have principal faults trending SW and dipping NE.

Structural Sections

Two cross sections were constructed using 2-D seismic information to analyze and illustrate the structure of the region. Their locations are shown in Figure 2.

Cross-section A in Figure 3 cuts the northern, central, and southern structural highs discussed above. The half-grabens between the highs are asymmetric, with their thickest parts generally adjacent to the principal faults to the southwest. The most important half-graben occurs between the southern and central highs. The postrift units (Quintuco and Centenario Formations) show a regional thickening to the southwest toward the center of the basin, and in some cases show a distortion related to the synrift faults. In this section, it is clear that the uppermost units of the sequence have a synclinal curvature just above the corresponding half-graben. This is common throughout the region and can be utilized to trace the axis of the principal half-grabens, even when deep seismic information is poorly defined.

Cross-section B in Figure 3 crosses the southern and central highs further to the northwest (Fig. 2). As in section A, the principal half-graben occurs between the southern and central highs, the sag and foreland units show a regional thickening to the southwest toward the center of the basin, and a local collapse occurs above each half-graben. The central high seems to act as a hinge between the principal grabens to the northeast and southwest.

Timing of Deformation

All the faults on the map in Figure 2 show evidence for important activity during the synrift stage (pre-Cuyo Group). They controlled the shape and position of the principal Triassic half-grabens. Because later movements on these faults are very small and difficult to analyze using 2-D seismic information, 3-D seismic lines were employed to study post-Triassic activity on the principal faults.

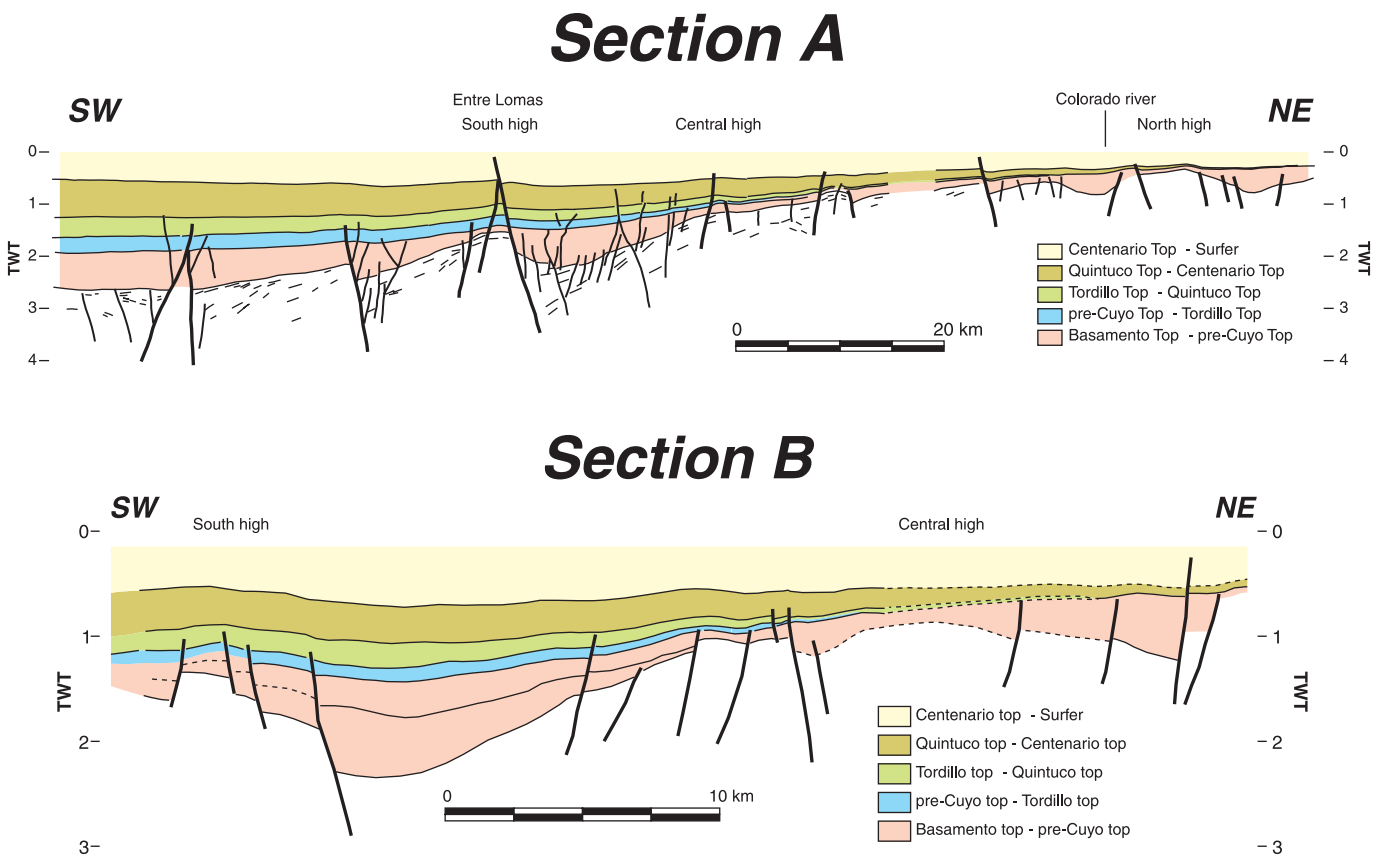

Figure 3. Cross sections of the region constructed using two-dimensional (2-D) seismic information. See location in Figure 2. TWT—two-way traveltime.

As an example, Figure 4 shows a 3-D seismic line from Bajo del Piche (see Fig. 2 for location), where three principal faults, labeled BP1, BP2, and BP3, can be seen. The first, BP1, is one of the major faults of the region. It bounds the northeastern side of the southern high (Entre Lomas high) and lies southwest of the principal half-graben in the region. This fault was only active during the synrift stage. In contrast, fault BP2, on the southwestern limit of the southern high, was not as important during the synrift period, but continued to move until at least the Cretaceous. The principal motion on this fault occurred during the Triassic and then diminished, becoming smaller during the Upper Jurassic (up to the time of the Tordillo Formation) and even smaller during the Cretaceous (up to time of the Rayoso Formation).

The timing information from all of the faults that were analyzed in the region is illustrated in Figure 5. The four maps sequentially show faults that were active up until the Late Jurassic (Tordillo Formation), the Lower to Middle Cretaceous (Centenario Formation), the Upper Cretaceous (Neuquén Group), and those that are affecting the present surface. Comparing Figures 2 and 5A, one can see that almost all the synrift faults developed during the Triassic were active up until the end of the deposition of the Tordillo Formation in the Late Jurassic. This pattern is also supported by well information. As an example, Figure 6 shows the thickness of the principal units in two contiguous wells, one over a horst and the second over a half-graben (see Fig. 2 for location). The thicknesses of the Lower to Middle Cretaceous units below the Late Jurassic Tordillo Formation increase to the south, following the regional slope of the basin. In contrast, the thickness of the Tordillo Formation increases to the north, following the local slope of the half-graben and showing that this half-graben was active in the Late Jurassic.

INTERPRETATION

Deformation after Synrift Stage

The origin of the anticlines that affect the postrift units in this part of the Neuquén Basin is considered below. An important observation is that the postrift units above the highs or anticlines are generally thicker than those in the troughs or synclines to the northeast, indicating that the deformation must be postsedimentation. Three possible deformational mechanisms that may explain the present configuration are shown in Figure 7: tectonic inversion, normal fault reactivation, and differential subsidence related to differential compaction. The main problem

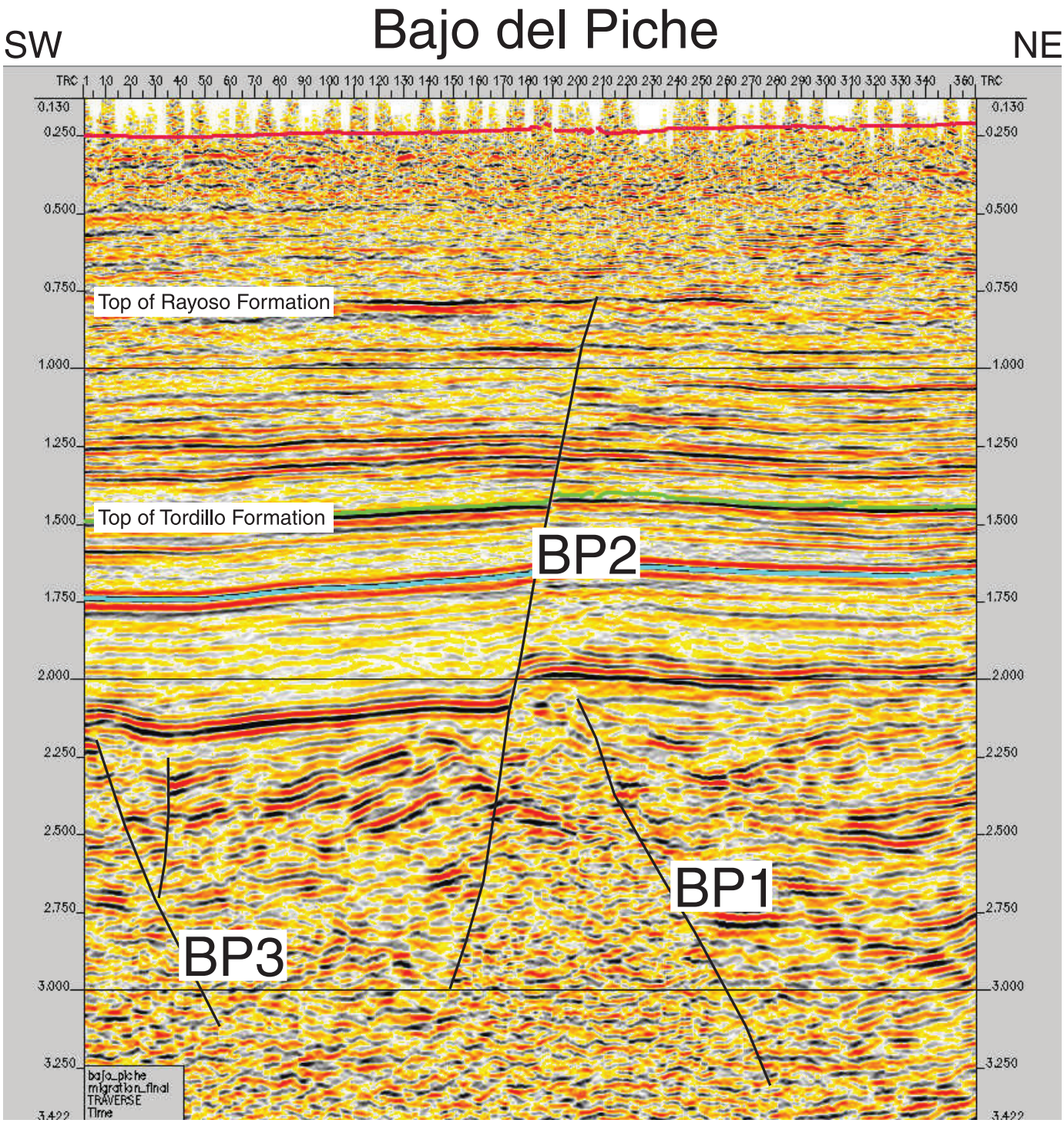

Figure 4. Structure of Bajo del Piche based on a three-dimensional (3-D) seismic line. Principal faults BP1, BP2, and BP3 are indicated. See Figure 2 for location.

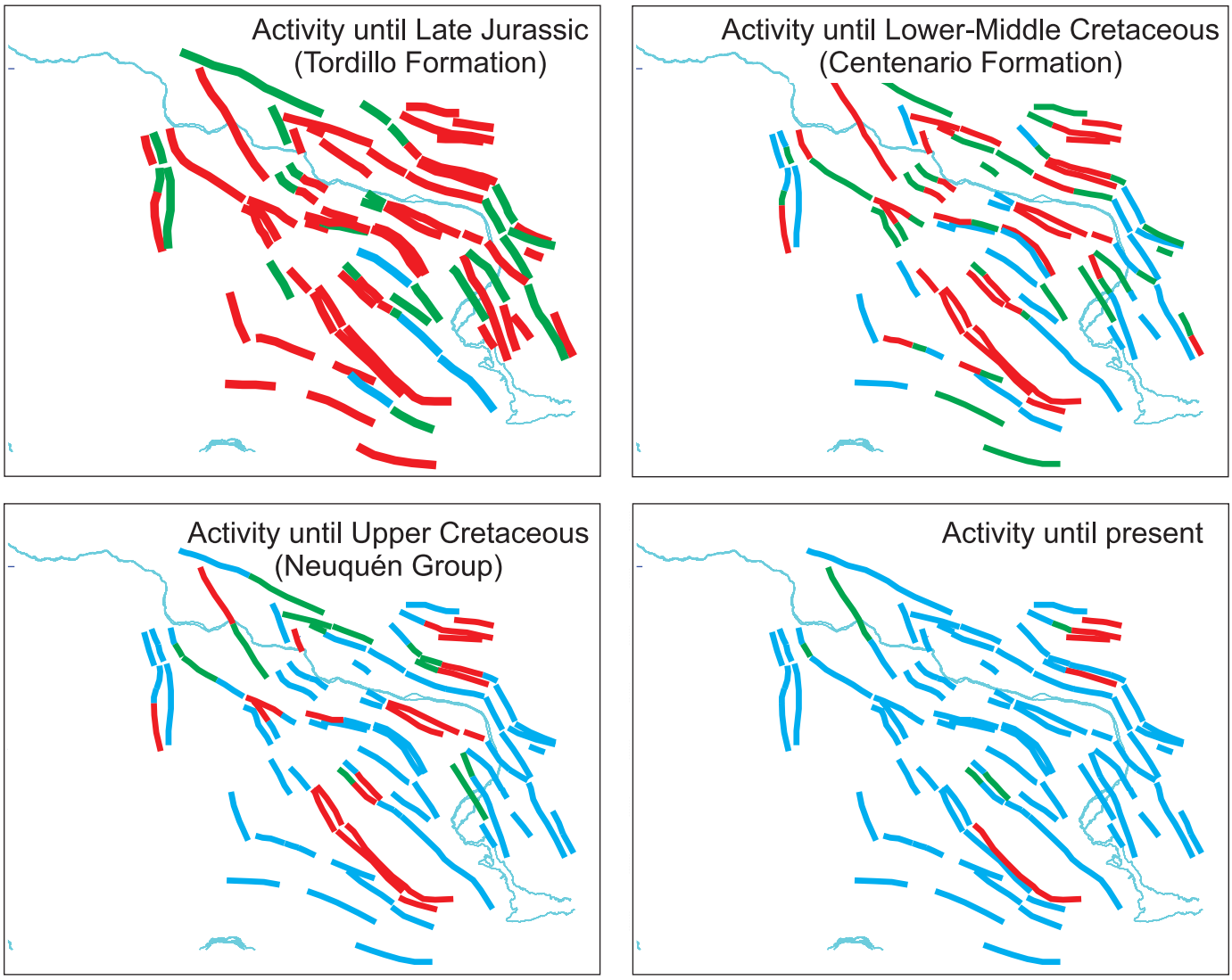

Figure 5. Maps showing the faults that report activity until the Late Jurassic (Tordillo Formation), Lower to Middle Cretaceous (Centenario Formation), Upper Cretaceous (Neuquén Group), and faults that are affecting the present surface. Red traces indicate fault activity, green traces indicate fold activity, and blue traces indicate no activity in the period. Each map represents the same area and structure of Figure 2.

is to establish the regional level of a unit (level of the unit before deformation). In the first case in Figure 7A, the regional level is between the hinges of the synclines. In the cases in Figures 7B and 7C, the regional level must be in the hinge of the anticline.

Figure 8 shows theoretical separation diagrams for the three mechanisms illustrated in Figure 7. These diagrams show plots of the separation from the regional level that a postrift unit acquires during deformation (dashed line) compared to the original shape of the synrift unit (gray line). For the case analyzed here, we constructed a separation diagram based on the principal units in cross-section A in Figure 3. A tracing of the principal units is shown in Figure 9. The regional level for each unit is arbitrarily placed in the anticline hinges (PC—pre-Cuyo Group, T—Tordillo Formation, Q—Quintuco Formation, C—Centenario Formation).

The central part of the section was selected to make the separation analysis. Figure 10 shows the resulting diagram for all of the markers; the thickness of the entire synrift unit is shown as a reference. A direct relation between the separation from regional levels of the postrift units and synrift thickness can be observed. A comparison between Figure 10 and the theoretical diagrams in Figure 8 shows that the separation curves in Figure 10 are most like the differential subsidence case in Figure 8A. The model for tectonic inversion can be dismissed, since Figure 10 shows exactly the opposite of what is seen in Figure 8C, and no evidence for tectonic inversion was observed in the seismic lines. The reactivation of normal faults model cannot be rejected based on these analyses, since the separation diagram in Figure 8B is similar to that for differen-

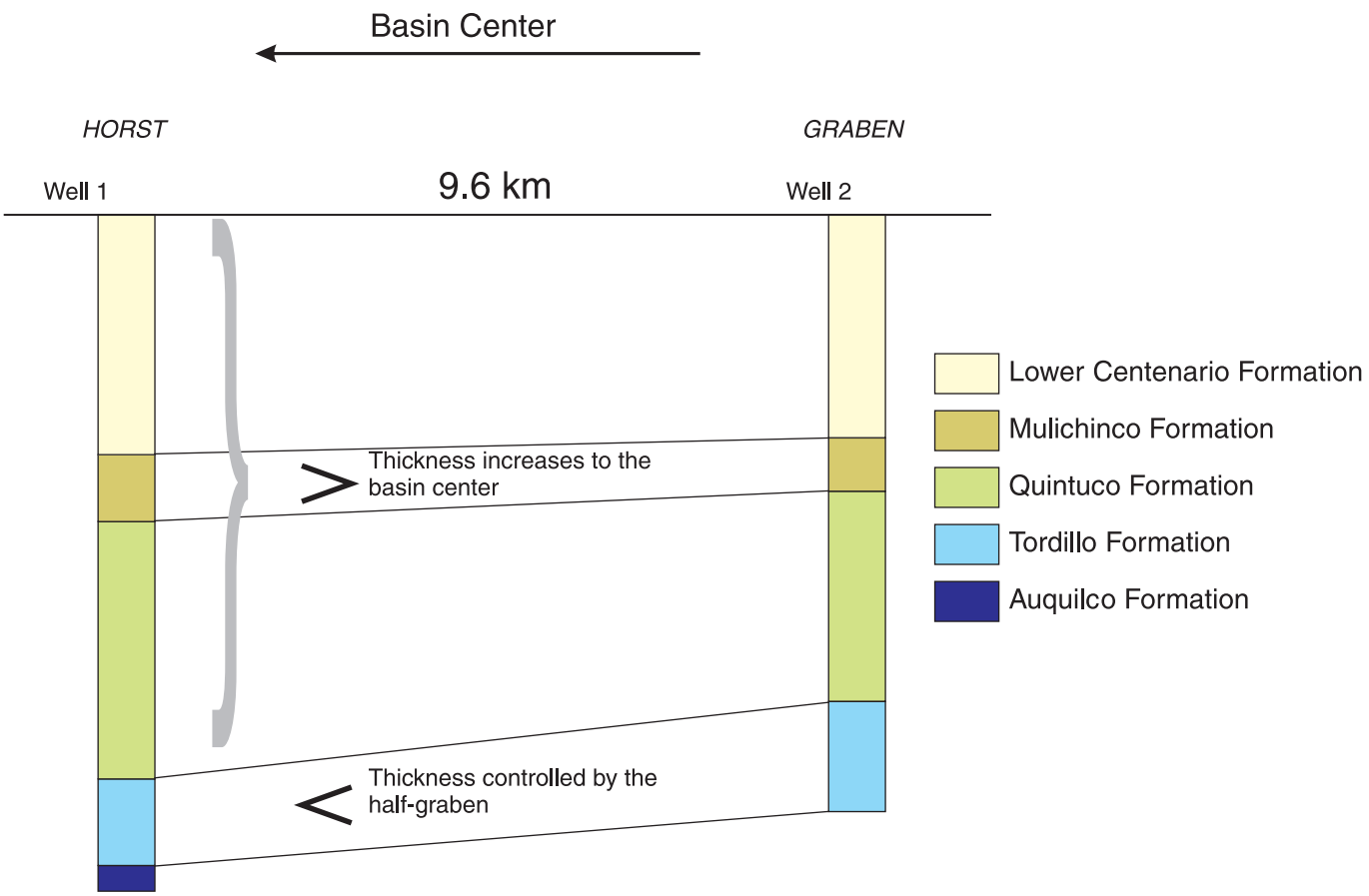

Figure 6. Variation of the thickness of the principal units in two contiguous wells: 1 and 2. Well 1 is over a horst and is south of well 2, which is over a half-graben. Note that the thickness of the Tordillo Formation increases to the north, following the local slope of a half-graben, whereas the thickness of the overlying Lower to Middle Cretaceous units increases to the south, following the regional slope of the basin. See Figure 2 for location of wells.

tial subsidence in Figure 8A, and there is evidence for fault reactivation all over the region.

As seen in Figures 8A and 8B, the main difference in the theoretical diagrams for differential subsidence and reactivation of normal faults is that the internal shape of the half-graben is followed by the separation curve in the differential subsidence case. In the case of normal fault reactivation, only the boundaries of the half-graben control the shape of the separation curve. In Figure 10, we can see that the shape of the separation curves mimics the shape of the half-grabens, especially the main one. As such, differential subsidence is the most probable mechanism to explain structural highs seen in the upper units.

Figure 6 shows that the thicknesses of units above the Tordillo Formation are greater in the high (horst) and smaller in the trough (graben) to the northeast. This is a common case for the uppermost units in other parts of the region, implying that differential subsidence took place after the formation of these units. This observation creates a problem for the differential subsidence model, because it is more intuitive to think that differential subsidence acts continuously. In the following, we show how this thickness relation between the highs and troughs can be explained using a continuous mechanism.

Theoretical Simulation of Differential Subsidence

A qualitative numerical simulation of the differential subsidence mechanism was preformed for cross-section A using the discrete element model of Cundall and Starck (1979) implemented by Zlotnik (2002) software AsBolinhas®. In the model, the rocks are simulated by individual circular elements that are separated from each other by frictional surfaces. A spring concept is used to join the individual elements to simulate a cohesive material. Each element and each spring is given physical properties (size, density, stiffness, etc.), and a statistical combination of these characteristics gives the material physical properties (density, Young modulus, Poisson coefficient, cohesion, internal friction, etc.).

Two simplified simulations of the half-grabens were performed, one without springs (noncohesive material; Fig. 11)

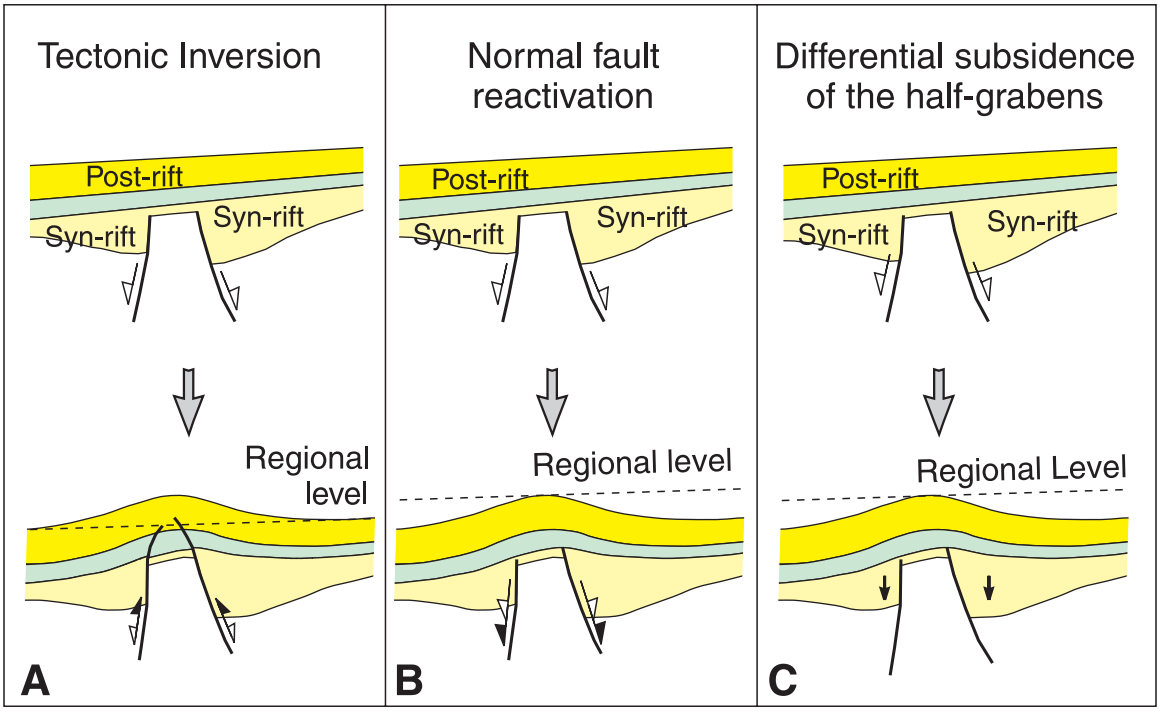

Figure 7. Three different mechanisms of deformation to arrive at the present configuration were evaluated: tectonic inversion, normal fault reactivation, and differential subsidence. RL—regional level.

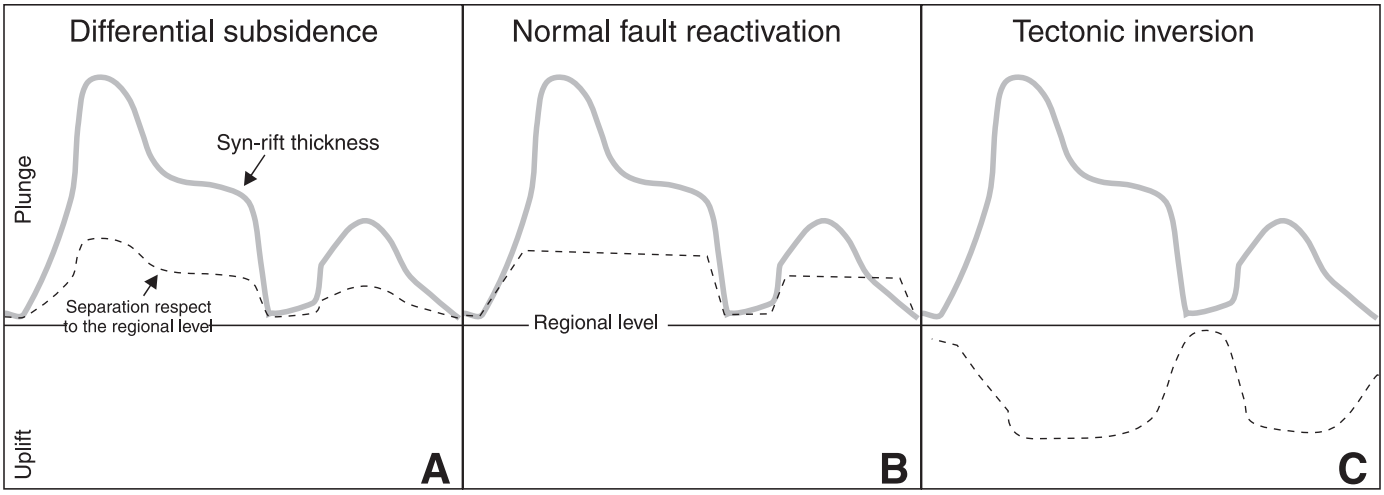

Figure 8. Theoretical separation diagrams are shown for the three mechanisms evaluated. These diagrams plot the separation from regional level that a postrift unit acquires during deformation (dashed line) in comparison to the shape of a synrift unit (gray line).

and the other with springs (cohesive material; Fig. 12). In both, schematic half-grabens were separated by a structural high that represents the Entre Lomas high in section A (Fig. 3). The basement was not allowed to deform, and the faults that bound the half-grabens were constrained not to move during the simulation. Both models had a similar design with 36,000 elements, and each ran for several days on a personal computer. Differential subsidence occurred in both models.

Figure 11A shows the results of the noncohesive simulation, in which anticlines of postrift material developed over the structural highs. Figure 11B shows the separation diagram for one layer in the model. A distinctive feature of the model is that the separation from the regional level occurred smoothly over the structural highs. Figure 12A shows the results of the cohesive simulation. In contrast to the noncohesive simulation, faults grew upward from the original synrift boundaries and cut

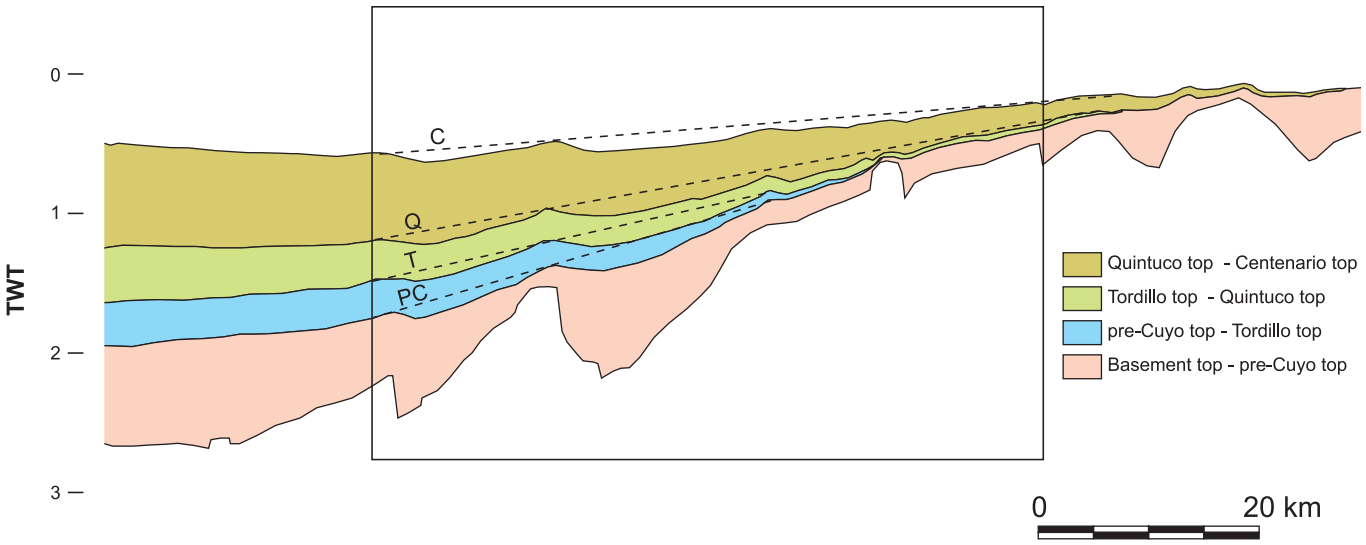

Figure 9. Tracing of the principal stratigraphic units in cross-section A in Figure 3. The regional level for each unit is arbitrarily placed in the anticlinal hinges. Abbreviations: PC—pre-Cuyo Group, T—Tordillo Formation, Q—Quintuco Formation, C—Centenario Formation.

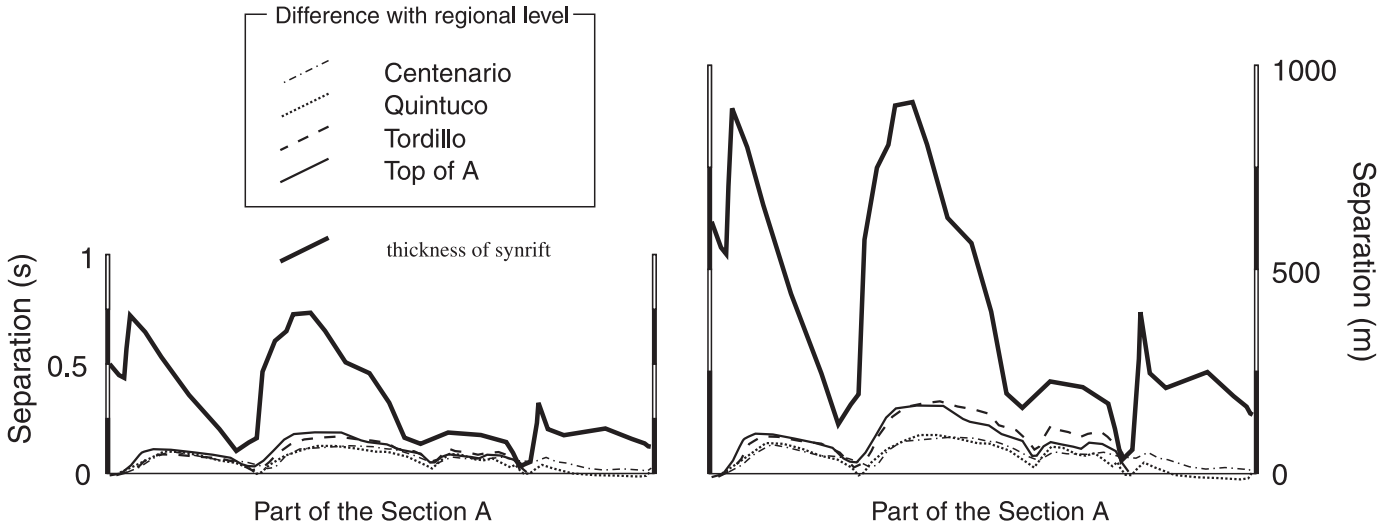

Figure 10. Resulting separation diagram for all the markers shown in Figure 9; the thickness of synrift unit is indicated as a reference. The scale on the left shows thickness, measured by two-way traveltime (TWT) in seconds, on a seismic line. The separation scale on the right shows the thickness transformed to distance using a regional velocity law.

the lowermost sag sequence. The diagram in Figure 12B shows an abrupt separation just above the synrift faults. The elements that broke springs during the simulation are shown in black in Figure 12A to emphasize the upward fault propagation that occurred in the synrift faults.

The separation diagram in Figure 10, based on cross-section A (Fig. 3), is more similar to that for the cohesive simulation in Figure 12 than for the noncohesive simulation in Figure 11. The analysis shows that some of the faults that cut the sag faces can be explained by fault propagation due to differential subsidence alone. No extensional tectonic mechanism is needed.

Evaluation of Differential Subsidence Mechanism

In order to evaluate the viability of differential subsidence as a generalized mechanism for the region, we decompacted the fill of the half-graben to the northeast of the Entre Lomas high. The shape of the half-graben is compared to three different decompaction curves for the top of the Tordillo Formation in Figure 13. The three curves are based on different porosity and compaction coefficients. Assuming a fill of 70% sandstone and 30% shale, the shape of the top of the Tordillo Formation marker is most easily restored to a planar outline using a porosity

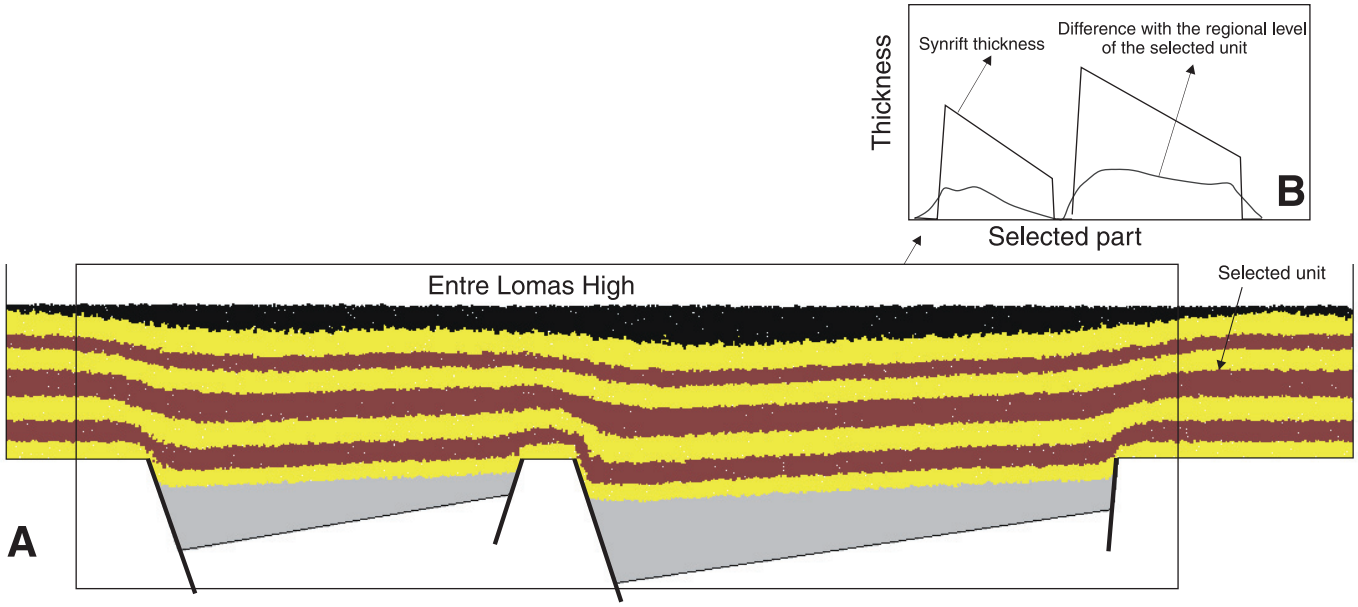

Figure 11. (A) Differential subsidence simulation with noncohesive material using distinct elements method. Anticlines of postrift units develop above the structural highs. (B) The separation diagram of a selected layer of the model.

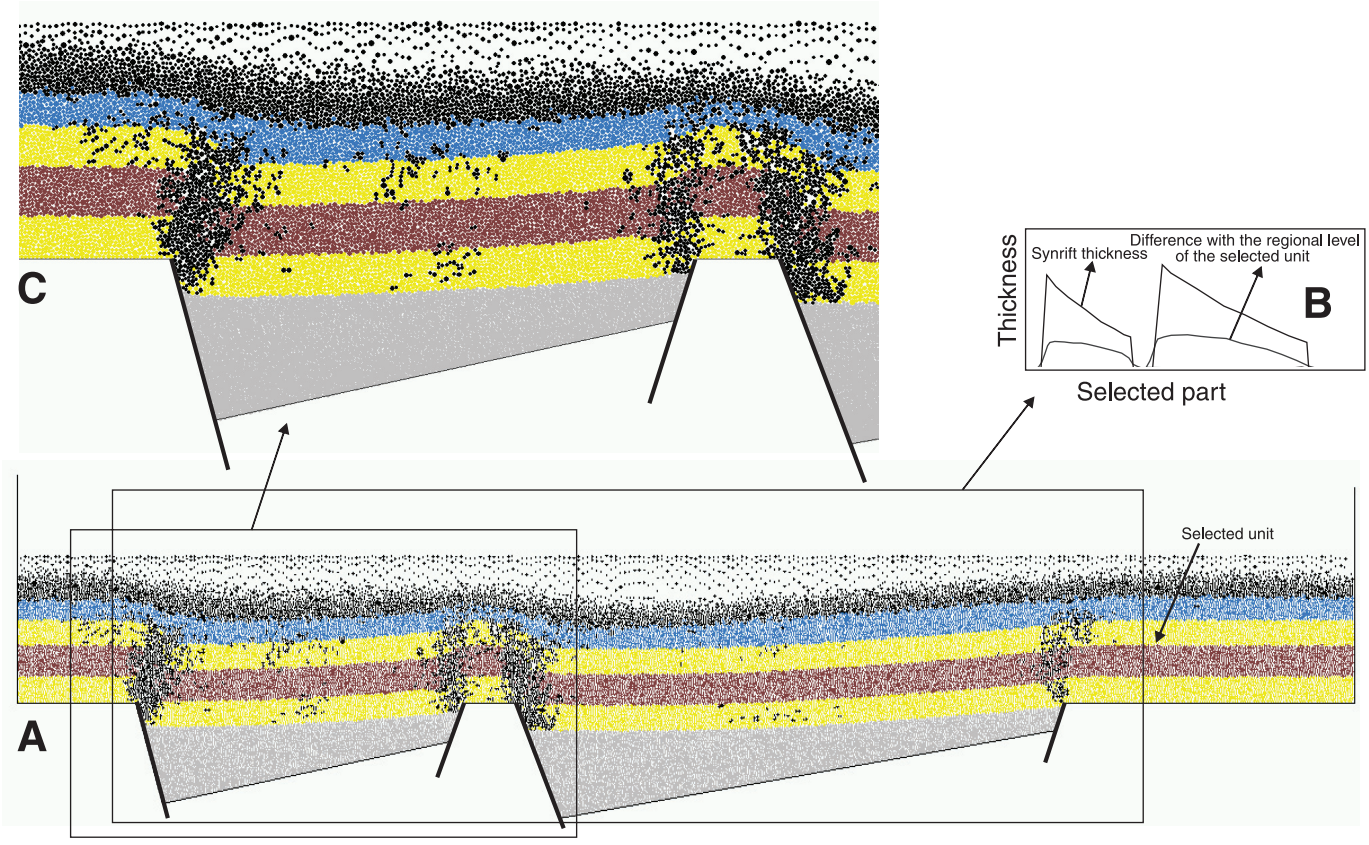

Figure 12. (A) Differential subsidence model using distinct elements method. Cohesive material was simulated using springs between elements. Anticlines of postrift units develop above the structural highs. (B) Separation diagram of a selected layer of the model. (C) Detail of the model where the elements that broke springs are blacked to illustrate fracturing and faulting nucleated above basement faults.

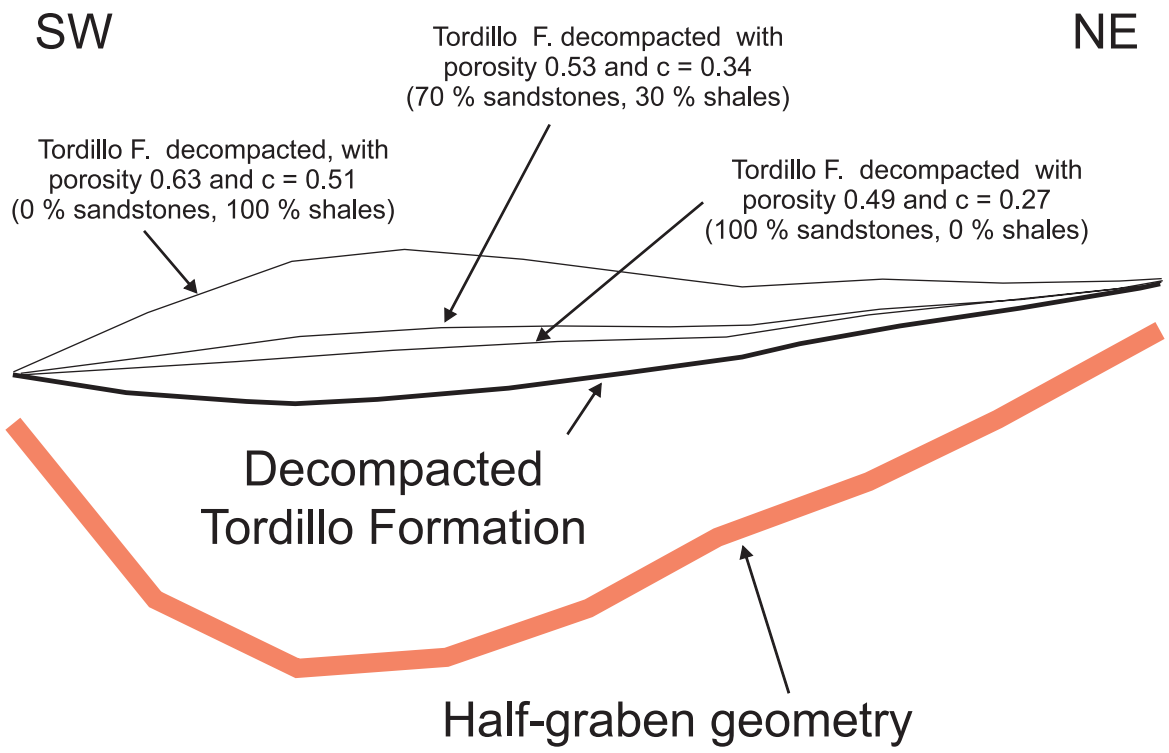

Figure 13. The shape of the half-graben to the northeast of the Entre Lomas high and curves of decompaction for the top of the Tordillo Formation for different porosity and compaction (c) coefficients (see reference in text).

of 53% and a compaction coefficient of 0.34 km^{-1}. However, the main purpose here is not to match the porosity and compaction coefficients of the half-graben filling, but to show that common synrift lithologies can produce differential compaction that is consistent with differential subsidence. Since the infilling of the pre-Cuyo half-grabens contains volcaniclastic rocks in some regions, we have done calculations that show that the change in volume produced by alternation of volcanic glass also contributes to differential compaction.

It is reasonable to think that differential compaction and subsidence should be linked in a continuous mechanism. A problem with such a linkage in the region of interest is that the uppermost postrift units (generally post-Tordillo Formation) are generally thicker over the highs than they are in adjacent troughs to the northeast. In other words, their postrift thicknesses are mainly controlled by regional slope, not by differential subsidence. As a first approximation, this relation indicates that differential subsidence occurred after deposition and did not control sedimentation rates.

A further analysis shows that the difference between the relative velocity of regional subsidence due to thermal effects and the relative velocity of local subsidence due to differential compaction controls the relative thicknesses of the sediments over the highs and in the troughs. Three cases are shown in Figure 14: (A) only regional subsidence; (B) differential subsidence slower than regional subsidence; and (C) differential subsidence faster than regional subsidence. The relative sediment thicknesses shown by the markers in Figure 14 demonstrate that when regional subsidence is faster than local subsidence, thickness increases toward the interior of the basin, and that when the reverse occurs, thickness increases in the troughs and decreases in the highs. In the cases where differential subsidence is occurring (Figs. 14B and 14C), smooth anticlines develop over the basement highs and smooth synclines over the basement troughs. The case in Figure 14B can be used to explain the geometry and sedimentation of the postrift units above the Tordillo Formation, and the case in Figure 14C, to explain those of the lower sag units up to the Tordillo Formation. In this way, we can explain the geometries and sedimentation pattern of the postrift units in the study region by continuous differential subsidence.

The difference between the discrete reactivation of normal faults and continuous differential subsidence models is significant for the evolution of the region. Given a differential subsidence model, basement structure exerts a control on sedimentation on all units above the basement, as well as the distribution of Mesozoic to Holocene fluvial paths. Basement control in the sedimentation of postrift units can be clearly seen until the Upper Jurassic (Tordillo Formation). We can see this by comparing the paleogeographic reconstruction of Cazau and Melli (2002) for the Sierras Blancas Formation (Tordillo Formation equivalent) with the synrift structural map in Figure 2 and noting that the

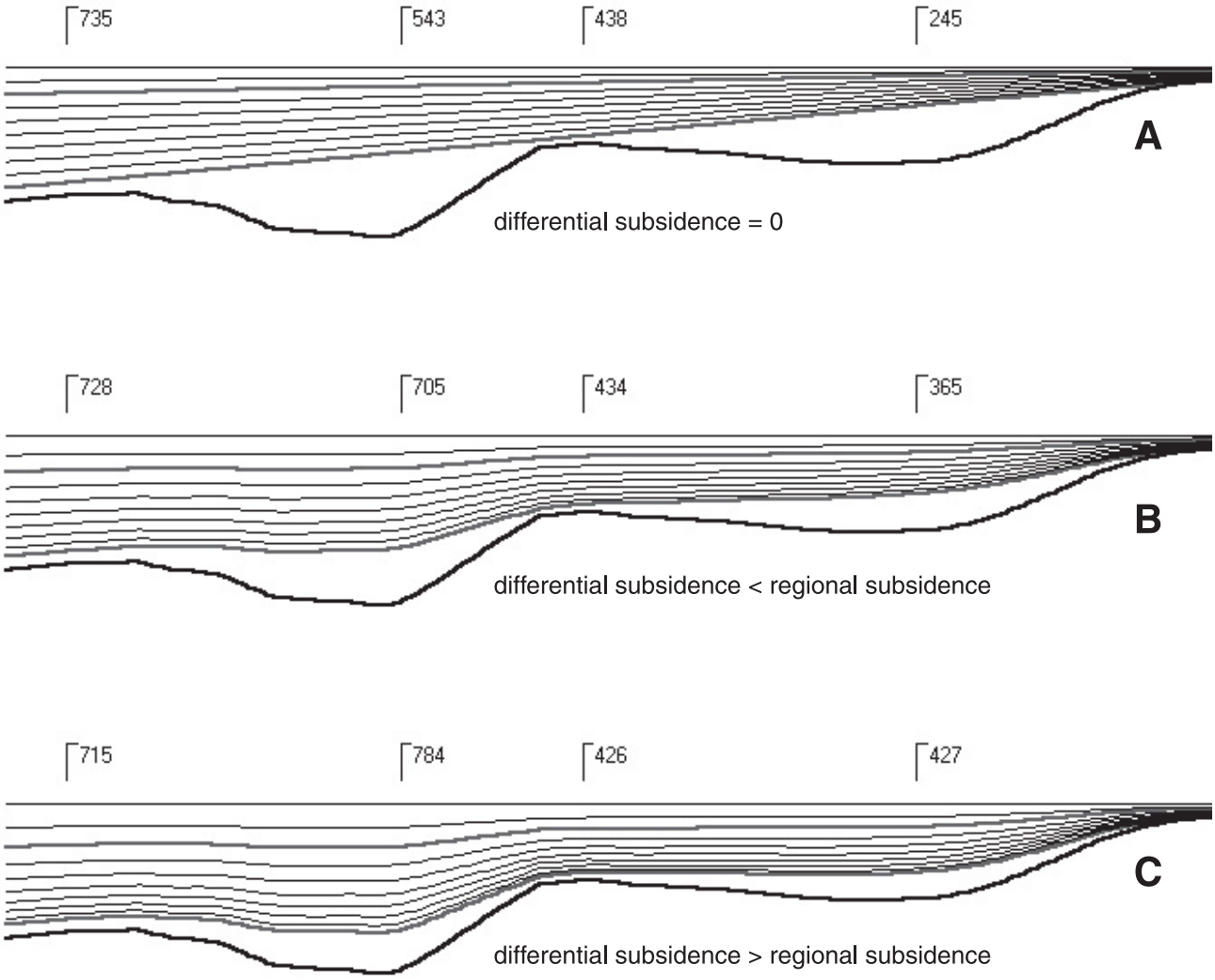

Figure 14. Relative rates of regional and local subsidence. Three cases are shown: (A) there is no differential subsidence (local subsidence); only regional subsidence is acting; (B) the differential subsidence is slower than the regional subsidence; and (C) the differential subsidence is faster than the regional subsidence.

principal rivers either parallel principal faults or transfer zones (Fig. 15). 3-D seismic data provide clear evidence for such control up until the Lower Cretaceous (Quintuco Formation). Later, the situation is less clear, because seismic evidence is poor. Nevertheless, evidence for basement control comes from the part of the present trace of the Colorado River and other modern fluvial courses that follow principal alignments of synrift faults or transfer zones.

CONCLUSIONS

We have analyzed the synrift structure of the northeastern region of the Neuquén Basin and produced an integrated regional map showing the location of the half-graben faults and transfer zones. The faults show a NW trend and generally dip to the NE or SW. Those that accommodate the main half-grabens are mostly NE-dipping. The transfer zones trend to the NE and divide the principal faults into segments that are shorter than 20 km.

The half-grabens and principal faults that affect the region developed in the synrift stage in the Upper Triassic to Lower Jurassic. During the subsequent sag stage, the activity of the principal synrift faults controlled sedimentation until at least the deposition of the Tordillo Formation in the Upper Jurassic. We suggest that this synrift activity was due to differential subsidence related to differences in compaction coefficients between the synrift deposits and basements rocks. In the Lower Jurassic, the velocity of local subsidence due to compaction was higher than the velocity of regional thermal subsidence. This relation subsequently inverted, and regional subsidence became faster.

We did not find any evidence to support tectonic inversion

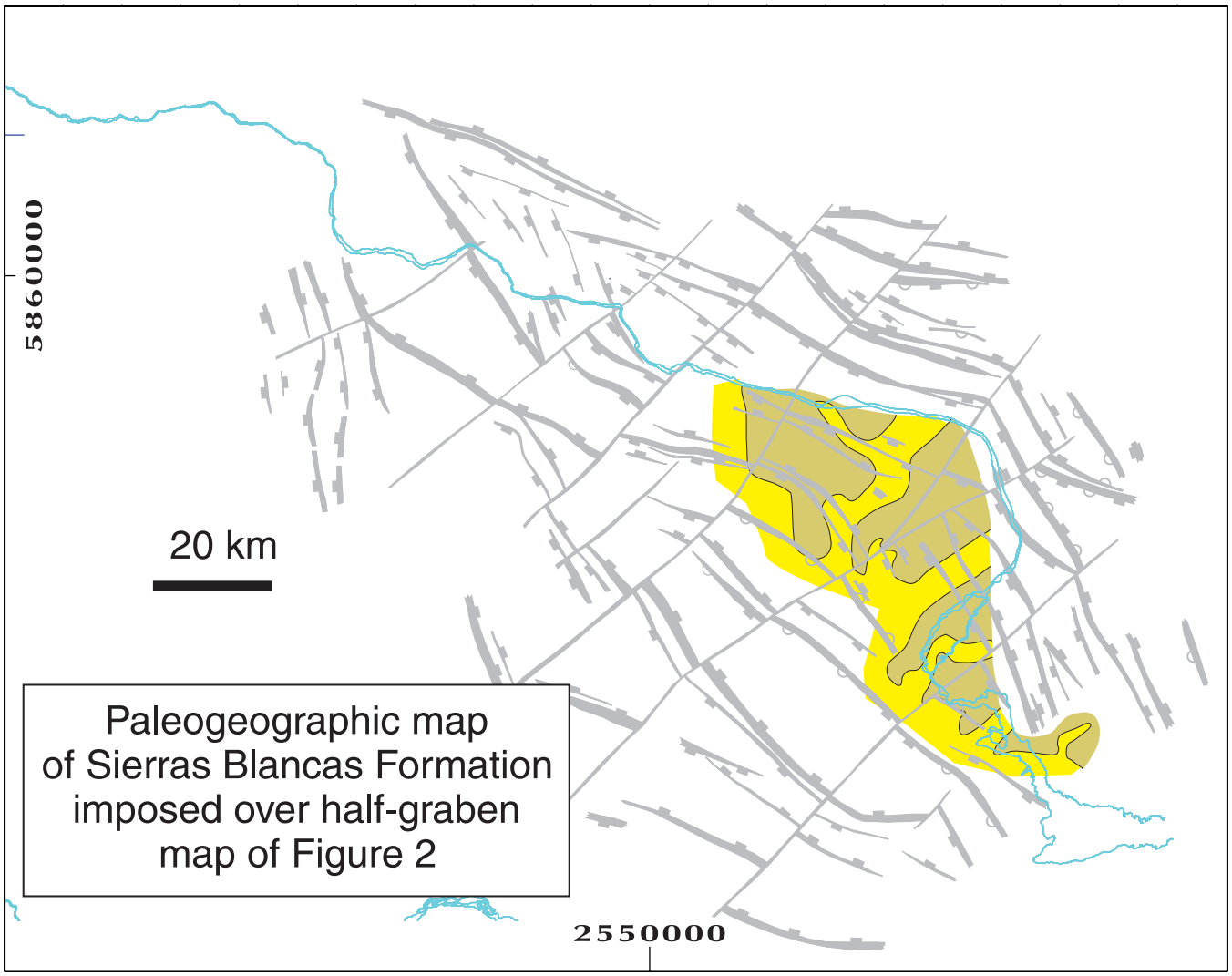

Figure 15. Paleogeographic reconstruction of Sierras Blancas Formation (Cazau and Melli, 2002) superimposed on the synrift structural map in Figure 2. Note that the principal fluvial courses are parallel to either the principal faults or the transfer zones. Sediment accumulation areas are shown in yellow and emergent areas in gray. Rivers were parallel to yellow trends.

as the mechanism that produced the anticlines and synclines in the northeastern region of the Neuquén Basin. In contrast, tectonic inversion related to transpression in the Jurassic played an important role in developing the structures to the south and southwest, in the region of the Huincul Ridge (Dorsal Neuquina) (Veiga et al., 1999; Mosquera, 2002; Pángaro et al., 2002). Similarly, tectonic inversion that initiated in the Upper Cretaceous played an important role in the development of the fold-and-thrust belt in western Neuquén and south Mendoza (Zapata et al., 1999; Kozlowski 1996; Manceda and Figueroa, 1995). The differences between the study area and the other regions can be reconciled by their relative locations (see Fig. 1).

The typical structure of the study region in the northeastern region of the Neuquén Basin consists of anticlinal highs and synclinal troughs that developed in postrift sedimentary sequences. We propose that a relatively simple differential subsidence model can explain their origin. No regional extension is needed to reactivate old normal faults or produce new ones. All of the structures in the Mesozoic to early Tertiary sequences can be explained by continuous subsidence controlled by differential compaction between synrift deposits and basement rocks.

ACKNOWLEDGMENTS

This work was founded by Repsol YPF, Universidad de Buenos Aires, Fundación Antorchas grants to Ernesto Cristallini and Renata Tomezzoli, and *Consejo Nacional de Investigaciones Científicas y Técnicas* grants to Ernesto Cristallini and Renata Tomezzoli. Special thanks are due to Estanislao Kozlowski and an anonymous reviewer.

REFERENCES CITED

Bettini, F.H., 1984, Pautas sobre cronología estructural en el área del Cerro Lotena, Cerro Granito y su implicancia en el significado de la Dorsal del Neuquén, Provincia del Neuquén, *in* Noveno Congreso Geológico Argentino: Actas, v. 2, p. 342–361.

Cazau, L., and Melli, A., 2002, La Formación Sierras Blancas en el noreste de la Cuenca Neuquina, *in* V Congreso de Exploración y Desarrollo de Hidrocarburos (Mar del Plata): electronic publication, CD-ROM.

Cundall, P.A., and Starck, D.L., 1979, A discrete numerical model for granular assemblies: Geotechnique, v. 29, no. 1, p. 47–65.

Dalmayrac, B., Laubacher, G., Marocco, R., Martinez, C., and Tomasi, P., 1980, La chaine Hercynienne d'Amérique du Sud: Structure et évolution d'un orogène intracratonique. Sonderdruck a.d.: Geologische Rundschau, v. 69, no. 1, p. 1–21, doi: 10.1007/BF01869020.

Kozlowski, E., 1996, Geología estructural de la zona de Chos Malal, Cuenca Neuquina, Argentina, *in* XIII Congreso Geológico Argentino y III Congreso de Exploración de Hidrocarburos: Actas, v. 1 p. 15–26.

Manceda, R., and Figueroa, D., 1995, Inversion of the Mesozoic Neuquén rift in the Malargüe fold-thrust belt, Mendoza, Argentina, *in* Tankard A.J., Suarez S., R., and Welsink, H.J. eds., Petroleum basins of South America: American Association of Petroleum Geologists Memoir 62, p. 369–382.

Mosquera, A., 2002, Inversión tectónica Jurásico inferior en el sector central de la dorsal de Huincul, área Los Bastos, *in* V Congreso de Exploración y Desarrollo de Hidrocarburos (Mar del Plata): electronic publication, CD-ROM.

Orchuela, I.A., Ploszkiewicz, J.V., and Viñes, R.F., 1981, Reinterpretación structural de la denominada "Dorsal de Huincul," *in* Octavo Congreso Geológico Argentino: Actas, v. 3, p. 281–293.

Pángaro, F., Veiga, R., and Vergani, G., 2002, Evolución tecto-sedimentaria del área de Cerro Bandera, Cuenca Neuquina, Argentina, *in* V Congreso de Exploración y Desarrollo de Hidrocarburos (Mar del Plata): electronic publication, CD-ROM.

Ploszkiewicz, J.V., Orchuela, I.A., Vaillard, J.C., and Viñes, R.F., 1984, Compresión y desplazamiento lateral en la zona de Falla de Huincul, estructuras asociadas, Provincia del Neuquén, *in* Noveno Congreso Geológico Argentino (Bariloche, Buenos Aires): Actas, v. 2, p. 163–169.

Ramos, V.A., 1984, Patagonia: Un continente Paleozoico a la deriva?, *in* Noveno Congreso Geológico Argentino (Bariloche, Buenos Aires): Actas, v. 2, p. 311–325.

Ramos, V.A., 1988, Tectonics of the Late Proterozoic–early Paleozoic: A collisional history of southern South America: Episodes, v. 11, no. 3, p. 168–174.

Tomezzoli, R.N., 2001, Further palaeomagnetic results from the Sierras Australes fold and thrust belt, Argentina: Geophysical Journal International, v. 147, p. 356–366, doi: 10.1046/j.0956-540x.2001.01536.x.

Veiga, R., Lara, M.E., and Bruveris, P., 1999, Distribución de hidrocarburos sobre el margen externo en una cuenca de tras-arco. Ejemplos en la cuenca Neuquina, Argentina: Boletín de Informaciones Petroleras (BIP), v. 60 (Diciembre 1999), p. 142–164.

Zapata, T.R., Brissón, I., and Dzelalija, F., 1999, La estructura de la faja plegada y corrida Andina en relación con el control del basamento de la cuenca Neuquina: Boletín de Informaciones Petroleras (BIP), v. 60, p. 112–121.

Zlotnik, S., 2002, Modelado numérico de estructuras y deformación de rocas mediante el método de elementos discretos [Trabajo Final de Licenciatura]: Buenos Aires, Universidad de Buenos Aires, 70 p.

MANUSCRIPT ACCEPTED BY THE SOCIETY 22 DECEMBER 2005